The performance simulation of air-cooled hydrogen storage device with plate fins

G. Mohan, M. Prakash Maiya and S. Srinivasa Murthy*

Refrigeration and Air Conditioning Laboratory, Department of Mechanical Engineering, Indian Institute of Technology Madras, Chennai 600 036, India

Abstract

This paper presents the heat and mass transfer performance of an air-cooled, multi-tube hydrogen storage device with plate fins and $LaNi_5$ as a hydriding alloy. The effects of number of tube rows, bed thickness and ratio of pitch distance to tube diameter (s/d) on the sorption performance of the device are reported. The influence of operating parameters such as air velocity and temperature on hydrogen sorption is also presented with emphasis on charging time and total system weight.

Keywords: $LaNi_5$; metal hydride; heat and mass transfer; hydrogen storage; plate fins

*Corresponding author:
ssmurthy@iitm.ac.in

Received 28 April 2009; revised 13 September 2009; accepted 4 December 2009

1 INTRODUCTION

Hydrogen storage devices are classified into liquid-cooled/-heated devices and air-cooled/-heated devices. Performance of liquid-cooled devices is widely investigated, whereas studies on air-cooled systems are relatively scarce. In these devices, heat and mass transfer augmentation are accomplished by suitable internal and external enhancements. Different internal heat transfer enhancements such as aluminium foam [1] and hydride compacts with binder systems such as aluminium/expanded graphite [2,3] are reported in the literature. In essence, they improve the effective thermal conductivity of hydride beds. MacDonald and Rowe [4,5] studied the effects of external convection on the thermodynamic behaviour in an air-cooled metal hydride tank. Their preliminary analysis confirmed the significance of external enhancement structures such as fins on overall heat transfer performance. This was verified by a numerical model, which revealed that when hydrogen is discharged by a pulsed mass flow rate demand, a finned tank is able to maintain a higher supply pressure.

Two common types of fins envisaged for the heat transfer augmentation in metal hydride devices include radial fins and plate fins. A recent study by the authors [6] dealt with the performance simulation of tubular storage device with radial fins. Compared with radial fins, plate fins are simple, compact, economic and rugged. Moreover, a multi-tubular storage device with plate fins is expected to perform better than a bundle of individual radial-finned tubes. The present paper deals with the sorption characteristics of tubular hydrogen storage devices with plate fins giving due importance on charging time and system weight.

2 THE PHYSICAL MODEL

Figure 1 illustrates a tubular metal hydride storage device with plate–fins and cylindrical tubes. The tubes are made up of stainless steel and are sufficiently strong to withstand the mechanical and thermal stresses during hydrogen sorption within the alloy bed. Porous sintered filters of cylindrical shape are located centrally within the hydride bed for uniform distribution of hydrogen. Annular region between the tube and filter is filled with hydrogen storage alloy. The plate fins are made up of aluminium, which ensures good heat transfer properties at low weight. All tubes are similar and spaced uniformly in a staggered configuration. Air is passed uniformly over the fins to remove the heat generated during the sorption process.

The above-mentioned configuration is adopted in the present study because it is well known that heat dissipated by the fin surface for a fixed fin volume is higher when the tubes are arranged in equilateral triangular configuration [7]. The tube bundle may be considered as an array of similar triangular cells in a 2D plane. The geometric definition of triangular cell is representative of its hydrogenation performance under specified operating conditions and known as the fundamental triangular cell as illustrated in Figure 2.

Important geometric parameters used to characterize the fundamental triangular cell of the above-mentioned configuration include bed thickness (b, in m), tube diameter (d, in m) and s/d ratio (where s refers to pitch distance, in m). Each paramater corresponds to a particular physical aspect of heat-controlled sorption process. Bed thickness at specified thermal conductivity controls the hydride bed heat transfer. Tube diameter and s/d ratio determine the external convective heat

International Journal of Low-Carbon Technologies 2010, 5, 25–34

doi:10.1093/ijlct/ctp039 Advance Access Publication 22 January 2010

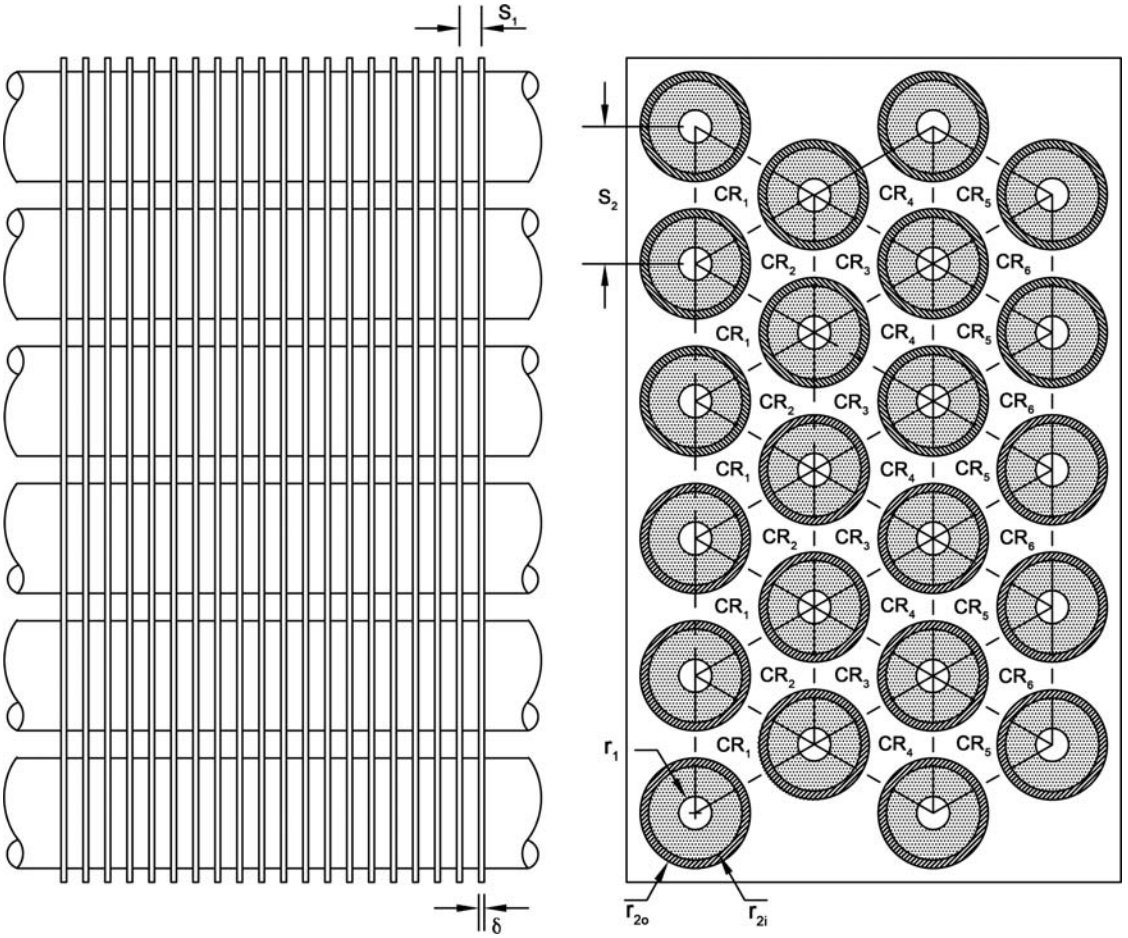

Figure 1. *Schematic of tubular metal hydride storage device with plate fins.*

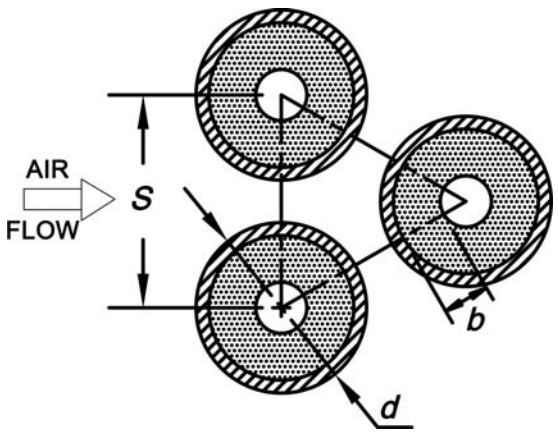

Figure 2. *Schematic of fundamental triangular cell of air-cooled hydrogen storage device with plate fins.*

transfer to the air stream. Packing the bundle of tubes at optimized *s*/*d* ratio and bed thickness ensures maximum heat transfer at specified operating conditions.

The heat and mass transfer performance of each cell depends on the corresponding conductive and convective heat transfer conditions. However, any two geometrically similar cells render same performance at identical operating conditions. Therefore, in a rectangular array of similar triangular cells, individual elements in any cell row (CR) deliver equal performance. The above statement holds true for tube rows, in which all tubes in any particular row show equal hydrogenation rates. However, the performance across different rows shows substantial variation in hydriding rates owing to variations in operating conditions.

3 PROBLEM FORMULATION

Simplified treatment of sorption process in metal hydride beds necessitate the following assumptions being made:

(i) Hydrogen is an ideal gas because the pressure within the bed is moderate.
(ii) Plateau slope and hysteresis factors of $LaNi_5$ are not large enough to have any significant effect on absorption [8]. Therefore, the effects of hysteresis and plateau slope for $LaNi_5$ are not accounted in simulation.

(iii) Pressure variation and associated gas movement inside the metal hydride bed is not very significant and the effect of convection inside the bed is negligible. $LaNi_5$ is a low-temperature hydriding alloy. Hence, radiation heat transfer inside the bed is not significant. Conduction is the prominent mode of heat transfer within the bed.
(iv) The hydride bed has uniform porosity. Brittle metal hydride materials upon cyclic hydrogenation asymptotically reach a minimum particle size [9]. Therefore, effect of powdering and variation in porosity is more pronounced in the early stages of absorption. After a certain number of charge–discharge cycles, the variation in porosity with time is insignificant.
(v) The hydride bed is assumed to be a homogeneous and isotropic porous media where permeability, effective thermal conductivity and mass diffusivity of bed are independent of position and direction.
(vi) Local thermal equilibrium exists between the gas and solid within the bed. Non-local thermal equilibrium effects are confined to the reactor wall and hydrogen filters. However, its overall effect on the performance of the device is minimal [10]. In most bulk portions of the bed, local thermal equilibrium is still valid. Therefore, it may be justified in simulation.
(vii) Thermo-physical properties such as thermal conductivity, dynamic viscosity and permeability of the bed are considered independent of bed temperature, pressure and concentration.

Important conservation equations valid in different computational domains are represented subsequently.

3.1 Mass balance of metal

Hydrogen entering the alloy bed through filters is absorbed and forms the metal hydride. Transient changes in hydride density are attributed to both absorption reaction and diffusive transport due to spatial variation in concentration. As listed under assumptions, a constant value of porosity is taken. Conservation of mass for the solid phase of the reactor in cylindrical coordinates is expressed in the following form:

$$(1-\varepsilon)\frac{\partial \rho_s}{\partial t} = (1-\varepsilon)\dot{m} + (1-\varepsilon)D\frac{1}{r}\frac{\partial}{\partial r}\left(r\frac{\partial \rho_s}{\partial r}\right) + (1-\varepsilon)D\frac{1}{r^2}\frac{\partial}{\partial \theta}\left(\frac{\partial \rho_s}{\partial \theta}\right) + (1-\varepsilon)D\frac{\partial}{\partial z}\left(\frac{\partial \rho_s}{\partial z}\right) \quad (1)$$

where ε is porosity, ρ density of the hydride (in kg m^{-3}), in amount of hydrogen absorbed (in kg m^{-3}s^{-1}), D diffusivity (in m^2 s^{-1}), r radial coordinate (in m) and θ is the polar coordinate (in rad).

Diffusivity D may be represented by the Arrhenius expression [11].

$$D = D_0 \exp\left(\frac{-H_a}{k_B T}\right) \quad (2)$$

where H_a is activation enthalpy (in eV), k_B Boltzmann constant (8.617×10^{-5}eV K^{-1}) and T is temperature (in K).

Transient variation in density on the left-hand side of Equation (1) is expressed as sum of four terms on the right-hand side. The first term represents the mass of hydrogen absorbed due to reaction. The remaining terms represent diffusive transport due to spatial gradients in concentration. Convection term is neglected.

3.2 Absorption kinetics

The amount of hydrogen absorbed is directly related with the reaction rate, and given by the following equation [12]:

$$\dot{m} = -C_a \exp\left(-\frac{E_a}{RT}\right) \ln\left(\frac{p}{p_{eq}}\right)(\rho_{sat} - \rho_s) \quad (3)$$

where C_a is a material-dependent constant, E_a is the activation energy of the material (in J mol^{-1}), ρ_{sat} is the density of hydride at saturation. The change in volume, if any, due to hydrogen absorption is not considered in the computation of density of the bed. The equilibrium pressure (P_{eq}, in pa) is determined by the van't Hoff relationship as given below:

$$\ln p_{eq} = A - \frac{B}{T} \quad (4)$$

where A and B are van't Hoff constants.

3.3 Energy balance of hydride bed

Heat generated due to exothermic reaction causes associated spatial temperature imbalances within the bed. Energy conservation equation of the bed could be expressed as given below:

$$(\rho c_p)_e \frac{\partial T}{\partial t} = k_e \frac{1}{r}\frac{\partial}{\partial r}\left(r\frac{\partial T}{\partial r}\right) + k_e \frac{1}{r^2}\frac{\partial}{\partial \theta}\left(\frac{\partial T}{\partial \theta}\right) + k_e \frac{\partial}{\partial z}\left(\frac{\partial T}{\partial z}\right) - (1-\varepsilon)\dot{m}\Delta H^0 \quad (5)$$

where c_p is specific heat (J kg^{-1} K^{-1}), t time (in s), k_e effective thermal conductivity (in W m^{-1} K) and ΔH^0 is the change in heat of formation (in J kg^{-1}).

Equation (5) assumes the existence of local thermal equilibrium between the solid and gas within the bed. Hence, the heat transfer between the two phases is omitted. Radiation heat transfer to the ambient is also neglected. Heat of formation of hydride represents the source term in the above equation.

Effective volumetric heat capacity is represented by the following expression:

$$(\rho C_p)_e = (\varepsilon \rho_H c_{pH} + (1-\varepsilon)\rho_s c_{ps}) \tag{6}$$

where H refers to hydrogen.

Effective thermal conductivity is expressed as given below:

$$k_e = \varepsilon k_H + (1-\varepsilon)\, k_s \tag{7}$$

Initial and boundary conditions: initially, the pressure and temperature of reactor bed are assumed to be uniform. Therefore,

$$p = p_0; \quad T = T_0; \quad \rho = \rho_0, \quad \text{at } t = 0 \tag{8}$$

The tube wall is impermeable to hydrogen, and heat flux continuity is applied at the inner wall. Convective mass flux boundary conditions are valid at the porous walls of the filter and it is assumed to be adiabatic for heat transfer. The boundary conditions may be expressed below in the following form:

$$\text{Filter tube wall } (t > 0): \quad \frac{\partial \rho_s}{\partial r} = 0; \quad p = p_{in}; \quad \frac{\partial T}{\partial r} = 0 \tag{9}$$

$$\text{Reactor tube inner wall } (t > 0): \quad \frac{\partial \rho_s}{\partial r} = 0; \quad \frac{\partial p}{\partial r} = 0 \tag{10}$$

$$-\boldsymbol{n} \cdot (-k_e \nabla T) = \boldsymbol{n} \cdot (-k_t \nabla T_t) \tag{11}$$

where P in is inlet pressure (in P_a), **n** is normal direction to the interface.

3.4 Energy balance of base tube and fin

Exothermic heat generated within the metal hydride bed is transferred to the fluid stream through the base tube and fin. Energy balance equations of the base tube and fin, respectively, are given below:

$$(\rho_t c_{pt}) \frac{\partial T_t}{\partial t} = k_t \left[\frac{1}{r} \frac{\partial}{\partial r} \left(r \frac{\partial T_t}{\partial r} \right) + \frac{1}{r^2} \frac{\partial^2 T_t}{\partial \theta^2} + \frac{\partial^2 T_t}{\partial z^2} \right] \tag{12}$$

$$(\rho_f c_{pf}) \frac{\partial T_f}{\partial t} = k_f \left[\frac{1}{r} \frac{\partial}{\partial r} \left(r \frac{\partial T_f}{\partial r} \right) + \frac{1}{r^2} \frac{\partial^2 T_f}{\partial \theta^2} + \frac{\partial^2 T_f}{\partial z^2} \right] \tag{13}$$

Initial and boundary conditions:

$$T_t = T_{t,0} \quad \text{and} \quad T_f = T_{f,0}, \quad \text{at } t = 0 \tag{14}$$

where T_t is tube temperature (in k) and T_f is fin temperature (in k).

Heat flux continuity conditions are valid at all interface boundaries. It may be expressed as given below:

$$\text{Tube/fin outer walls}(t > 0): \quad -\boldsymbol{n} \cdot (-k_t \nabla T_t) = \boldsymbol{n} \cdot (-k_g \nabla T_g + \rho_g c_{pg} \boldsymbol{u} T_g) \tag{15}$$

$$-\boldsymbol{n} \cdot (-k_f \nabla T_f) = \boldsymbol{n} \cdot (-k_g \nabla T_g + \rho_g c_{pg} \boldsymbol{u} T_g) \tag{16}$$

$$\text{Tube–fin interface}(t > 0): \quad -\boldsymbol{n} \cdot (-k_t \nabla T_t) = \boldsymbol{n} \cdot (-k_f \nabla T_f) \tag{17}$$

3.5 Momentum balance of air stream

Navier–Stokes equations describe the gas (air) flow through the finned tube flow passages. The density (ρ_g in kg m^{-3}) and viscosity (u_g in m s^{-1}) changes of air due to temperature variations are assumed to be constant.

$$\rho_g \frac{\partial u_x}{\partial t} = -\frac{\partial p}{\partial x} + \mu_g \left[\frac{\partial^2 u_x}{\partial x^2} + \frac{\partial^2 u_x}{\partial y^2} + \frac{\partial^2 u_x}{\partial z^2} \right] - \rho_g \left[u_x \frac{\partial u_x}{\partial x} + u_y \frac{\partial u_x}{\partial y} + u_z \frac{\partial u_x}{\partial z} \right] \tag{18}$$

$$\rho_g \frac{\partial u_y}{\partial t} = -\frac{\partial p}{\partial y} + \mu_g \left[\frac{\partial^2 u_y}{\partial x^2} + \frac{\partial^2 u_y}{\partial y^2} + \frac{\partial^2 u_y}{\partial z^2} \right] - \rho_g \left[u_x \frac{\partial u_y}{\partial x} + u_y \frac{\partial u_y}{\partial y} + u_z \frac{\partial u_y}{\partial z} \right] \tag{19}$$

$$\rho_g \frac{\partial u_z}{\partial t} = -\frac{\partial p}{\partial z} + \mu_g \left[\frac{\partial^2 u_z}{\partial x^2} + \frac{\partial^2 u_z}{\partial y^2} + \frac{\partial^2 u_z}{\partial z^2} \right] - \rho_g \left[u_x \frac{\partial u_z}{\partial x} + u_y \frac{\partial u_z}{\partial y} + u_z \frac{\partial u_z}{\partial z} \right] \tag{20}$$

where μ_g is dynamic viscosity of air (in P_a s).

3.6 Energy balance of air stream

The following equation describes the energy balance of air stream passing over the fin assembly. Conduction heat loss from the storage device is equal to the convective heat gain by the air stream.

$$(\rho_g c_{pg}) \frac{\partial T_g}{\partial t} = -(\rho_g c_{pg} u_x) \frac{\partial T_g}{\partial x} - (\rho_g c_{pg} u_y) \frac{\partial T_g}{\partial y} - (\rho_g c_{pg} u_z) \frac{\partial T_g}{\partial z} \tag{21}$$

Initial and boundary conditions:

$$T_g = T_{g,0} \quad \text{at } t = 0 \tag{22}$$

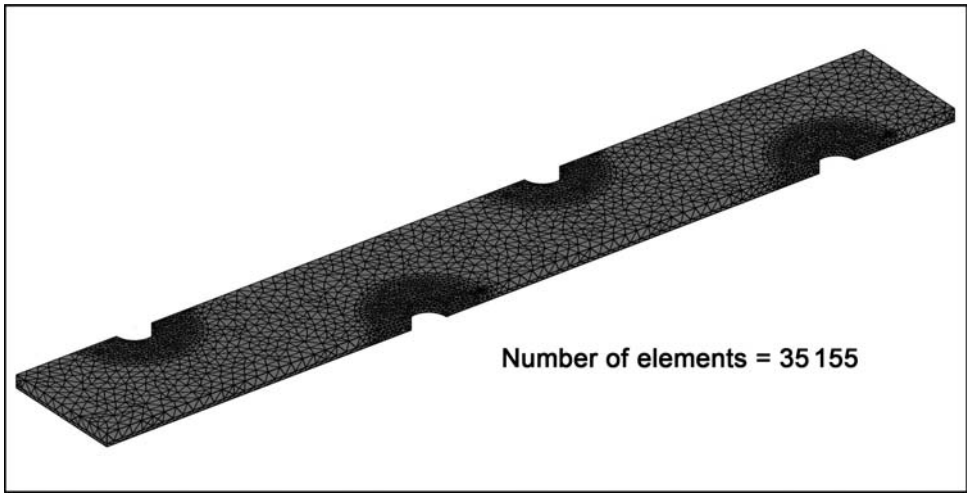

Figure 3. *Computational mesh of 3D model in COMSOL MULTIPHYSICS®.*

An appropriate rectangular prismatic sub-domain represents the fluid stream. Fluid velocity and temperature at the inlet of the sub-domain are known. Convective heat flux conditions are applied at the exit. Symmetry conditions are assumed at the exterior boundaries. No slip conditions are valid at the walls.

$$\text{Air inlet } (t > 0): \quad u_x = u_{\text{in}};\ u_y = 0;\ u_z = 0;\ T_{\text{g}} = T_{\text{g in}} \tag{23}$$

$$\text{Air exit } (t > 0): \quad p = p_0;\ q \cdot \boldsymbol{n} = \rho_{\text{g}} c_{\text{pg}} T_{\text{g}} \boldsymbol{u} \cdot \boldsymbol{n} \tag{24}$$

4 SIMULATION METHODOLOGY

The simulation of the metal hydride bed as per the above formulation is realized using COMSOL MULTIPHYSICS® commercial code. Symmetry of the physical model enables the resulting computational model to be less memory intensive. The metal hydride bed, base tube, fin and fluid stream are modelled as separate sub-domains. The model is drawn using AutoCAD® drafting package and duly imported for further processing. Relevant physics and material properties are applied to different sub-domains. The convection–diffusion, non-isothermal flow and general heat transfer modules define the mass, momentum and energy conservation equations, respectively. Suitable multi-physics coupling and boundary conditions needs to be defined at the physics settings. Once the physics of the problem is duly defined, a mesh of suitable element quality is generated with suitable control parameters. The resulting model after mesh generation is shown in Figure 3. Solving the model with a set of non-linear equations demands the application of time-dependent, iterative solvers for proper convergence. Generated data after post-processing provide sufficient insights into the hydriding characteristics of the device.

5 RESULTS AND DISCUSSION

$LaNi_5$, a well-documented storage material at low/moderate operating temperatures, is considered for the present simulation. The reaction rate of $LaNi_5$ is extremely fast and the alloy performance is limited by heat transfer in most cases. Reaction kinetics and thermo-physical properties of $LaNi_5$ are given in Table 1. Parameter ranges of geometric and operating parameters employed in the present simulation are given in Table 2.

5.1 Mechanism of hydrogen sorption

Air enters the finned-tube metal hydride device at specified temperature and velocity and passes through the intermediate passages before it leaves out of the bundle. While passing over the tubes and fins, the air stream picks up the heat generated within the hydride bed. Consequently, the air gets heated up progressively from the inlet to the exit and its temperature rises. In the meanwhile, hydriding takes place within the bed and the reaction in each tube is rate limited by the surrounding air temperature. Higher air temperature in the vicinity of the hydride bed leads to lower reaction rate and vice-versa. Therefore, the gradual temperature rise along the stream leads to gradual reduction in sorption rate in successive tube rows. Figure 4 depicts the temperature and concentration profiles of the storage device at different time intervals. The gradual variation of temperature and the corresponding differences in concentration at different tube rows may be observed in the surface plot. It may be observed further that the stream gets cooled up gradually with associated delay in charging in different tube rows downstream the air flow.

The hydrogen sorption during initial stages of reaction is dependent more on material than on heat transfer. The reaction kinetics of the material is invariably fast in the initial stages and the rate of temperature rise of hydride bed is found to be more drastic. Temperature rise is found to be severe near the filter. The extent of heat-affected zone gradually diminishes with time, indicating the increasing role of heat transfer. A lot of disparity may be observed among different tube rows in the rate of shrinkage of the high-temperature region. First row cools down much faster compared with other rows and a

Table 1. *Thermo-physical properties of $LaNi_5$ and hydrogen [11,13].*

Parameters	$LaNi_5$	Hydrogen
Density (kg m^{-3})	8200	0.0838 at NTP
Specific heat (J kg^{-1} K^{-1})	419	14 890
Effective thermal conductivity (W m^{-1} K^{-1})	1.2	0.12
Activation energy (J mol^{-1})	21179.6	—
Constants in Equations (2), (3) and (4)		
D_0 (m^2 s^-)	3.4×10^{-7}	—
C_a	59.187	—
A	12.99	—
B	3704.59	—
Activation enthalpy (eV)	0.29	—

Table 2. *Parameter ranges used in simulation.*

Parameter	Range
Initial temperature of hydride bed (K)	300
Temperature of hydrogen at inlet (K)	300
Supply pressure of hydrogen (bar)	15.0
Air temperature at inlet (K)	300
Face velocity of air stream (m s^{-1})	0.5–3.5
Bed thickness (mm)	2.5–6.5
Thickness of fin (δ, mm)	1
s/d ratio of tubes	1.25–2.5
Number of rows	2–4
Fin pitch (mm)	4

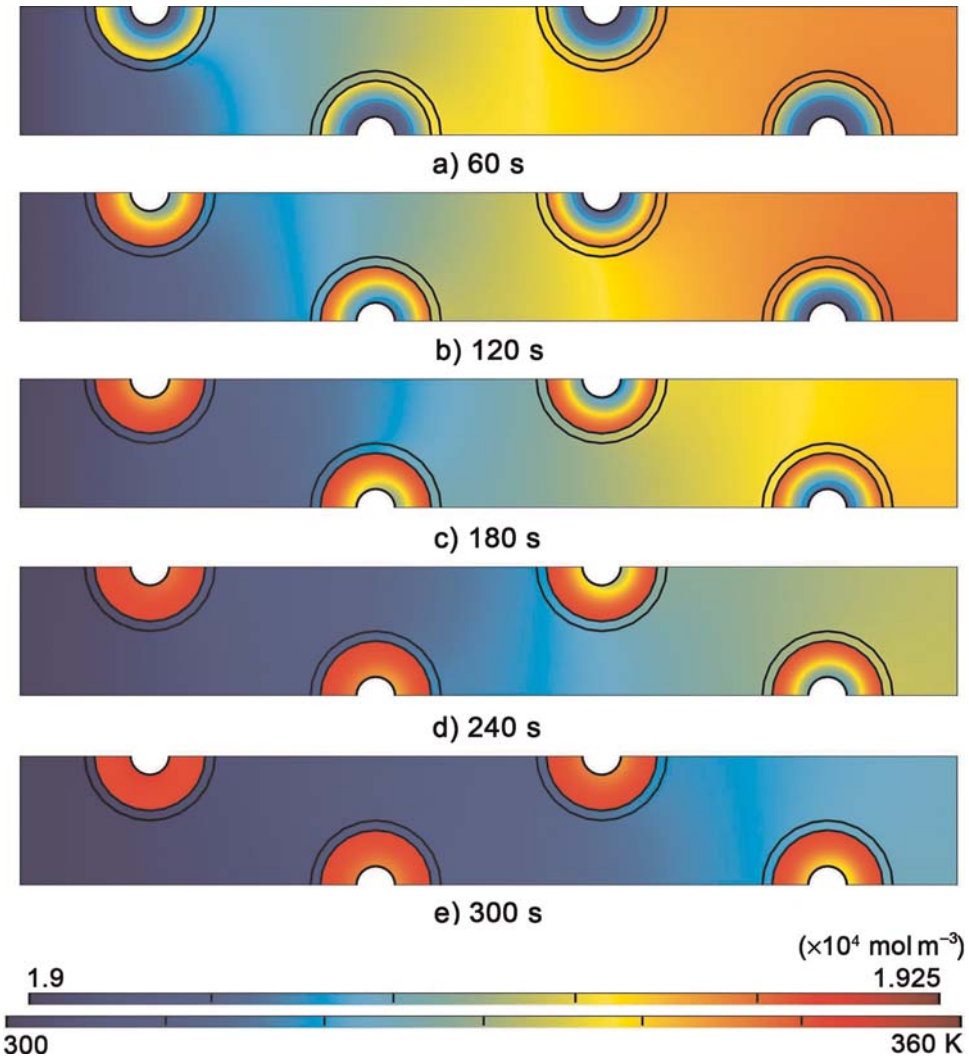

Figure 4. *Temperature profile of air and concentration profile of hydride bed at different time intervals* (p = *15 bar,* $T_{g,in}$ = *300K,* s/d = *2,* b = *5.5 mm,* u= *1 m/s).*

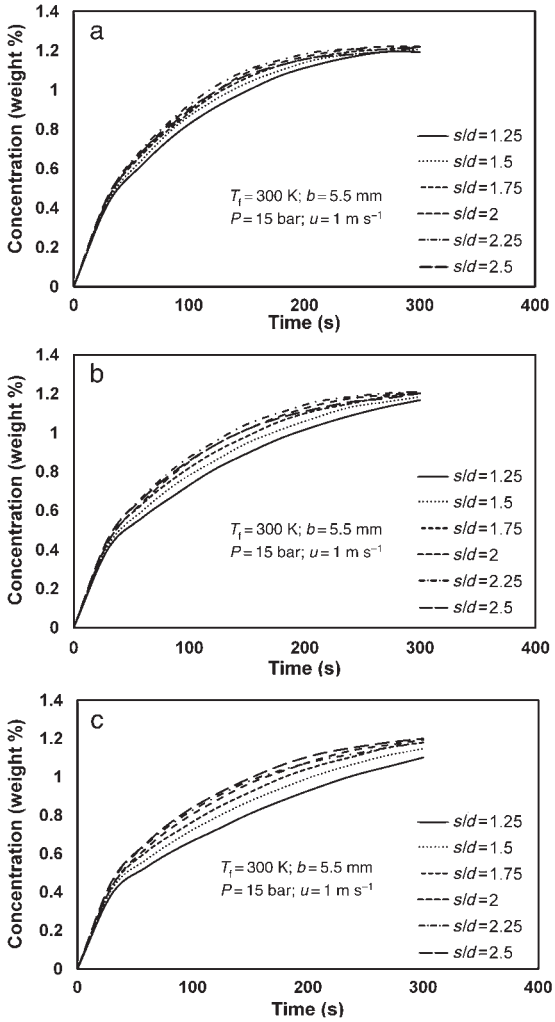

Figure 5. *Rate of hydriding of finned tube bundles arranged at different* s/d *ratios and number of rows; (a) two rows, (b) three rows and (c) four rows.*

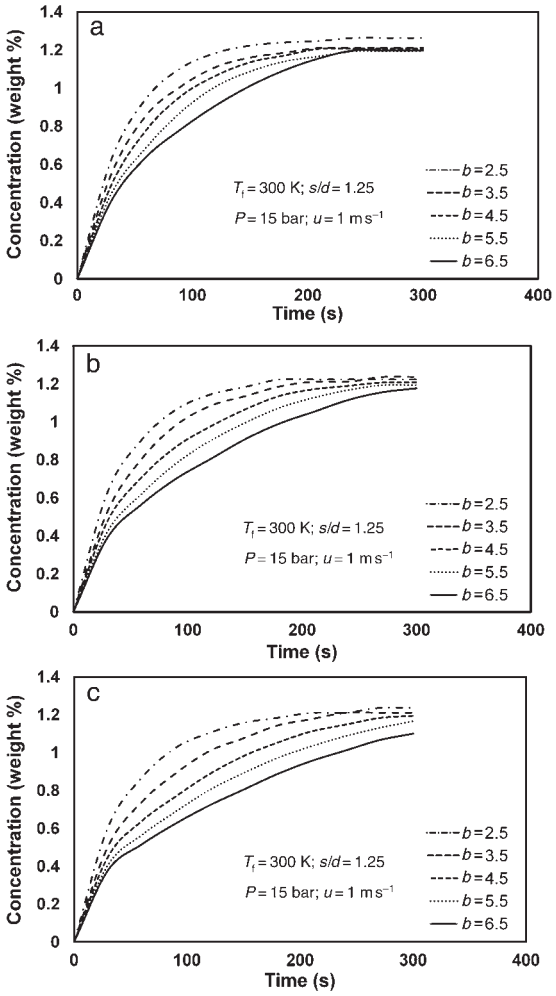

Figure 6. *Rate of hydriding of finned tube bundles at different bed thicknesses and number of rows; (a) two rows, (b) three rows and (c) four rows.*

gradual reduction in cooling rate may be observed among successive rows.

The impact of heat removal rate on hydriding is exemplified by the spatial variation of concentration with time. One may observe a growing reaction front, which progresses gradually from the tube wall to the filter. The rate of progress of the above front differs among different rows. The rate of traverse of the front is the highest in the first row followed by successive rows in order. Conversely, preceding rows get saturated much faster compared with successive rows down-stream. The relative rate of advance of the reaction front in different tube rows may be aptly substantiated with the heat transfer rate.

5.2 Effect of geometric parameters on hydrogen sorption

Figure 5 shows the effect of *s*/*d* ratio on the rate of hydrogen sorption in finned tube metal hydride device arranged in different rows. The convective transport of the rejected heat depends on the prevailing flow conditions within the flow passage. Reducing *s*/*d* ratio increases the mean fluid temperature inside the passage that reduces the overall heat transfer rate from the hydride bed. On the contrary, heat transfer coefficient on the air side increases when *s*/*d* ratio decreases [14]. However, its effect on hydriding is found to be marginal. Lower heat transfer rate lowers the hydriding rate. In essence, reducing *s*/*d* ratio reduces the hydriding rate of the device and requires higher charging time. Further, the temperature of the air increases progressively down-stream of the flow. As a result, the rate of hydriding decreases progressively for successive rows, with the first row exhibits the highest rate. For the above reason, arrangement of tubes with too many numbers of rows is not preferred unless space limitations play an important role. However, the disparity observed between different rows is either absent or marginal at the initial phases of reaction where it is controlled predominantly by the intrinsic kinetics of the storage alloy.

The effect of bed thickness on the rate of hydrogen sorption for the above device is shown in Figure 6. As already pointed

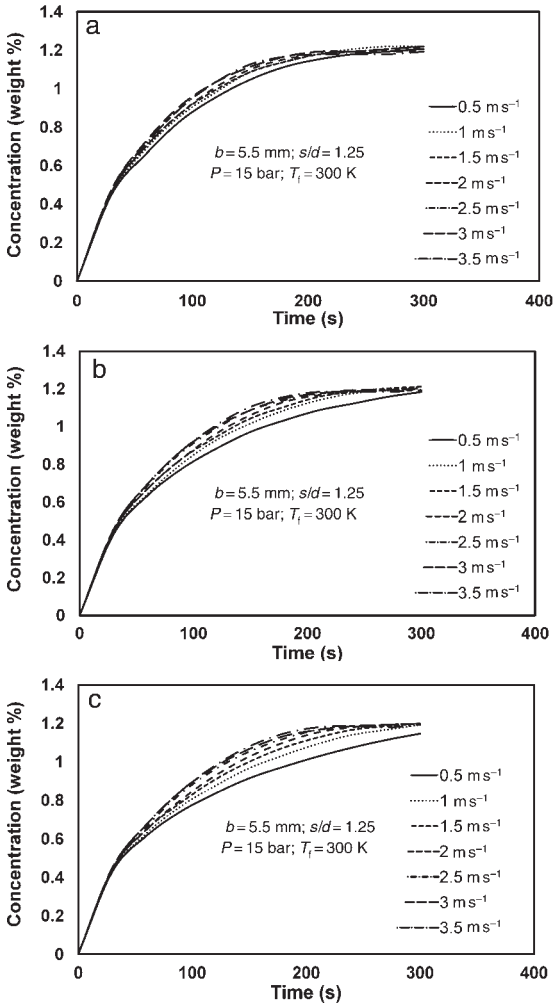

Figure 7. *Effect of air flow velocity on rate of hydriding of finned tube bundles arranged in different number of rows; (a) two rows, (b) three rows and (c) four rows.*

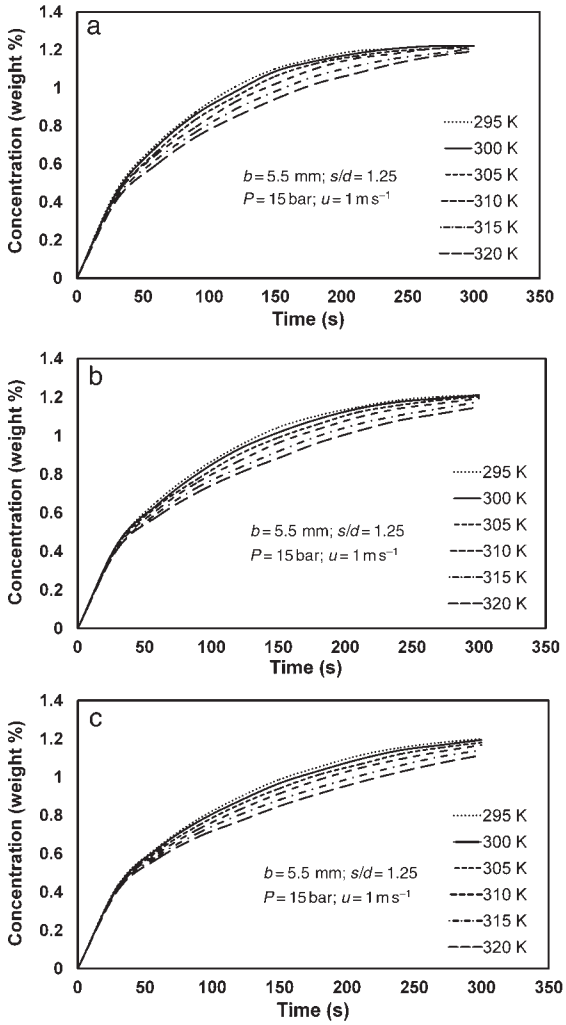

Figure 8. *Effect of inlet air temperature on rate of hydriding of finned tube bundles arranged in different number of rows; (a) two rows, (b) three rows and (4) four rows.*

out, hydriding in the initial stages is controlled by the intrinsic reaction kinetics and hence the difference is found to be marginal among different cases. Heat transfer become rate controlling in the subsequent stages of reaction where bed thickness plays an important role. Thicker beds offer higher thermal resistance compared with thinner ones. Therefore, heat transfer and hydriding rate in thicker beds are poorer than their thinner counterparts. Consequently, more charging time is required for thicker beds. Disparity in hydriding rates among different tube rows is evident in the present case as well. It owes further to the progressively lowered heat transfer performance in successive rows.

5.3 Effect of operating parameters on hydrogen sorption

As already discussed, reaction kinetics is the sole factor controlling the rate of hydriding during the initial phase of reaction whereas the rest of the reaction is controlled by heat transfer. Convective heat transport controls the rate of hydriding in air-cooled devices and it depends on the external flow conditions prevailing in the flow field. Effect of flow velocity on the convective heat transport and rate of hydriding is discussed in the following paragraphs.

Figure 7 shows the effect of flow velocity on the hydriding performance of the device. It may be observed that increasing the flow velocity is favourable for faster rate of hydriding. However, improvement is found to be marginal for higher velocities. It is due to the fact that external heat transfer is no longer a rate controlling factor beyond a certain flow velocity. The above observation further suggests the existence of a mutual correlation between the heat transfer characteristics of the hydride bed and the external convective flow. Arrangement of tubes in rows may be reasonable from the point of view of space limitations. However, the sorption performance deteriorates due to increased heat pick up and associated temperature

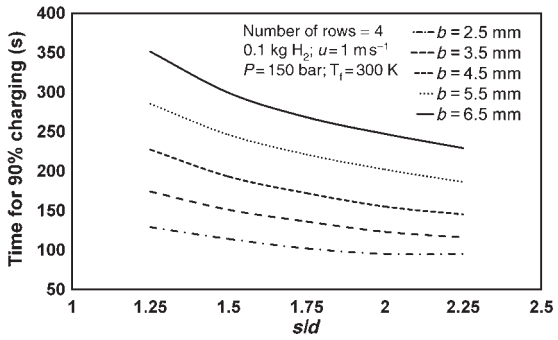

Figure 9. *Effect of* s/d *ratio on charging time at different bed thicknesses.*

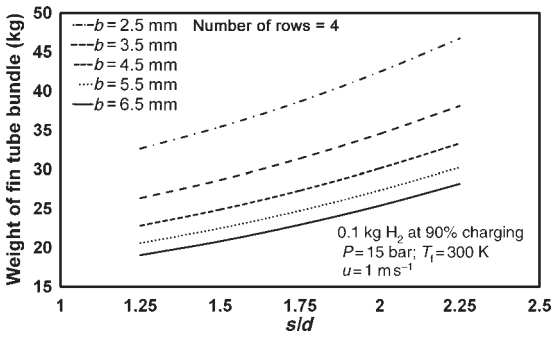

Figure 11. *Effect of* s/d *ratio on weight of the device at different bed thicknesses.*

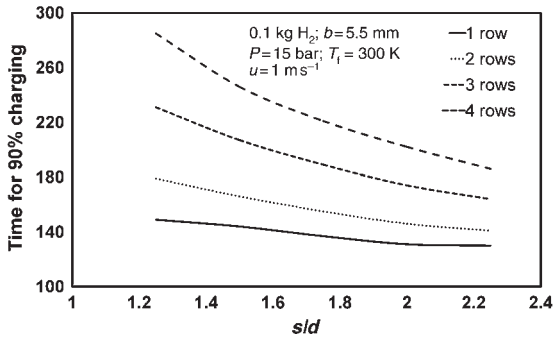

Figure 10. *Effect of* s/d *ratio on charging time for devices with different number of tube rows.*

rise of heat transfer media as it passes over the tubes. The above problem may be remedied to a certain extent with enhanced flow velocity.

Hydrogen sorption in metal hydride bed is controlled by the differential in supply pressure and equilibrium pressure. Increasing the bed temperature increases the equilibrium pressure. Heat gain by air at successive rows increases the temperature of the hydride bed and thereby decreases the sorption rate. Effect of inlet air temperature on the rate of hydrogen sorption at different number of tube rows is shown in Figure 8. Increasing the inlet temperature of air increases the hydride bed temperatures in each row. It decreases the hydriding rate and the effect is nearly uniform in all rows.

5.4 Effect of geometric parameters on charging time and system weight

The merit of a hydrogen storage device may be judged based on two important performance parameters, namely, charging time and system weight. Effect of geometric parameters on the above parameters for a typical case with storage capacity of 0.1 kg of hydrogen at 90% charging is discussed in the following paragraphs.

Effect of *s*/*d* ratio on charging time at different bed thickness for a finned-tube metal hydride device with four rows is shown in Figure 9. Charging time required in all different cases reduces as *s*/*d* ratio increases. The above result is in agreement with previous results, where the rate of hydriding increases with *s*/*d* ratio. Thicker beds require more charging time compared with their thinner counterparts. Further, the variation in charging time is more pronounced for thicker beds. The above effect may be attributed to the increased relevance of external heat transfer in thicker hydride beds.

Figure 10 shows the effect of *s*/*d* ratio on charging time for different number of tube rows. As explained earlier, heat pick-up of heat transfer fluid leads to progressively poor overall heat transfer in succeeding rows. Therefore, the device with more tube rows requires more charging time. Moreover, relevance of fluid temperature is increasingly felt in the last two rows, visibly affect the performance of storage devices with more number of tube rows.

Charging time and system weight are equally important factors in several mobile and portable applications. In most cases, they are mutually contradicting as the enhancement of one leads to loss of the other. Figure 11 shows the effect of *s*/*d* ratio on device weight at different bed thickness. An increase in *s*/*d* ratio reduces the charging time at the expense of additional system weight incurred due to larger fin area. Reducing the fin volume is found to be an effective strategy to reduce the overall system weight. Application of thinner fins may be effective in reducing the overall system weight, keeping the charging time unaffected. Bed thickness is the foremost factor in deciding the total system weight. Thinner beds at constant weight of alloy requires the device to be longer, leading to additional weight incurred due to tubes, filters and fins. The above effect seems apparent from the above figure. Therefore, the bed needs to be sized carefully without hampering the charging requirements.

6 CONCLUSIONS

Heat and mass transfer simulation of air-cooled, cylindrical, multi-tube metal hydride hydrogen storage device with plate fins is carried out with $LaNi_5$ as the storage alloy. The rate of hydrogenation of the device is affected by the combined influence of bed thickness and *s*/*d* ratio, indicative of the

mutual correlation between hydride bed heat transfer and convective transport of the rejected heat. Addition of multiple tube rows reduces the overall sorption performance of the device. Air velocity and temperature are two important operating parameters that control the sorption rate. Influence of s/d ratio and number of tube rows on hydriding is found to be less pronounced compared with bed thickness, but cannot be neglected. Bed thickness and tube diameter are two important geometric parameters that control the charging rate and system weight. Minimization of total system weight needs the optimization of above parameters at specified storage capacity, charging rate and space constraints for a given application.

FUNDING

The financial support from U.S. Army Communications – Electronics Research, Development and Engineering Center, and International Technology Center, Pacific are gratefully acknowledged.

REFERENCES

[1] Suda S, Komazaki Y, Kobayashi N. Effective thermal conductivity of metal hydride beds. *J Less-Common Met* 1983;**89**:317–24.

[2] Ron M, Gruen D, Mendelsohn M, *et al*. Preparation and properties of porous metal hydride compacts. *J Less-Common Met* 1980;**74**:445–8.

[3] Kim KJ, Montoya B, Razani A, *et al*. Metal hydride compacts of improved thermal conductivity. *Int J Hydrogen Energy* 2001;**21**:609–13.

[4] MacDonald BD, Rowe AM. Impacts of external heat transfer enhancements on metal hydride storage tanks. *Int J Hydrogen Energy* 2006;**31**:1721–31.

[5] MacDonald BD, Rowe AM. A thermally coupled metal hydride hydrogen storage and fuel cell system. *J Power Sources* 2006;**161**:346–55.

[6] Mohan G, Prakash Maiya M, Srinivasa Murthy S. Performance of air cooled hydrogen storage device with external fins. *Int J Low-Carbon Tech* 2009;**4**:265–81.

[7] Kundu B, Das PK. Optimum dimensions of plate fins for fin-tube heat exchangers. *Int J Heat Fluid Flow* 1997;**18**:530–7.

[8] Hydride Information Centre. Sandia National Laboratories, USA (http://www.hydpark.ca.sandia.gov).

[9] Ron M. The normalized pressure dependence method for the evaluation of kinetic rates of metal hydride formation/decomposition. *J Alloys Compd* 1999;**283**:178–91.

[10] Lloyd GM, Razani A, Kim KJ. Formulation and numerical solution of non-local thermal equilibrium equations for multiple gas/solid porous metal hydride reactors. *Trans ASME J Heat Transfer* 2001;**123**:520–6.

[11] Majer G, Kaess U, Bowman RC, Jr. Nuclear magnetic resonance studies of hydrogen diffusion in $LaNi_{5.0}H_{6.0}$ and $LaNi_{4.8}Sn_{0.2}H_{5.8}$. *Phys Rev B* 1998;**57**:599–603.

[12] Jemni A, Nasrallah SB. Study of two dimensional heat and mass transfer during absorption in a metal-hydrogen reactor. *Int J Hydrogen Energy* 1995;**20**:43–52.

[13] Dogan A, Kaplan Y, Veziroglu TN. Numerical investigation of heat and mass transfer in a metal hydride bed. *Appl Math Comput* 2004;**150**:169–80.

[14] Yan WM, Sheen PJ. Heat transfer and friction characteristics of fin-and-tube heat exchangers. *Int J Heat Mass Transfer* 2000;**43**:1651–9.